# A model compound for pyridinechalcone-based multistate systems. Ring Opening-Closure as the Slowest Kinetic Step of the Multistate.

Ambrósio Camuenho,[a] António J. Parola,[a],* Alfonso Alejo-Armijo,[a]
Ramesh Pandian,[b] Clara S. B. Gomes,[a] César A. T. Laia,[a] Fernando Pina[a],*

[a] LAQV-REQUIMTE – Laboratório Associado para a Química Verde, Departamento de Química, Faculdade de Ciências e Tecnologia, Universidade NOVA de Lisboa, 2829-516 Monte de Caparica, Portugal. email: ajp@fct.unl.pt

[b] Protein Structure-Function Research Unit, School of Molecular and Cell Biology, University of the Witwatersrand, South Africa

## Abstract

Anthocyanins and related flavylium derivatives exist in aqueous solution as a pH-dependent mole fraction distribution of species (a multistate system) with known biological activity. Introduction of nitrogen heterocycles in the flavylium core can lead to multistates with different constitution and increased activity. Compound **1**, a diethylamino derivative of 4-pyridinechalcone, was synthesized and characterized by X-ray crystallography, showing a pH-dependent reaction network similar to anthocyanins and related compounds. The several species present at the equilibrium multistate were fully characterized by $^1$H NMR and $^{13}$C NMR. The thermodynamics and kinetics of the multistate were studied through pH jumps followed by $^1$H NMR and UV-vis absorption including stopped-flow for the faster kinetic steps. In the parent 4-pyridinechalcone compound, protonation of the pyridine nitrogen for pH<4 prevents formation of the flavylium cation. In compound **1**, the first protonation takes place in the diethylamino substituent and in acidic medium, two new flavylium derivatives, a single (2<pH<4) and a double (pH<1) positively charged species, in equilibrium with protonated hemiketal, *cis* and *trans* chalcones, have been characterized. Differently from anthocyanins and related compounds, experimental evidence for an unexpected very slow (0.0003 s$^{-1}$) ring opening-closure between the hemiketal and the *cis*-chalcone (tautomerization) was achieved.
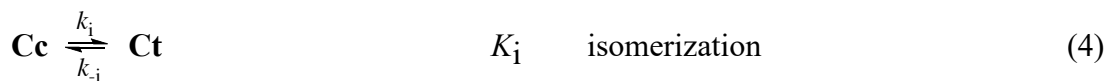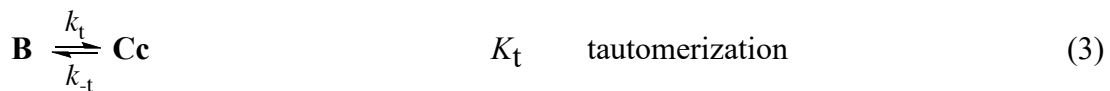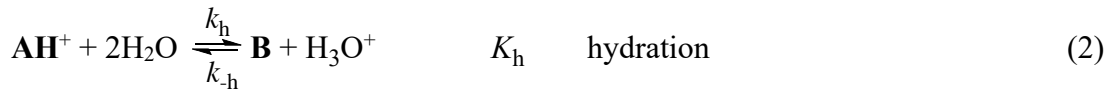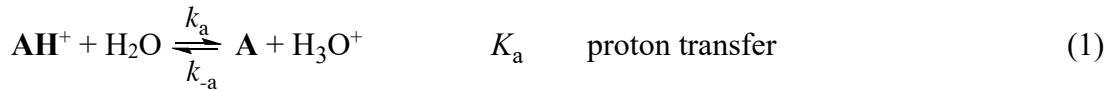
**Introduction**

Anthocyanins in solution give rise to several species connected through pH-dependent equilibria, as exemplified in Scheme 1. This multistate of species is followed by other families of related compounds such as anthocyanidins,[1,2] pyranoanthocyanins,[3] deoxyanthocyanins,[4,5] naphthoflavylium,[6] styrylflavylium,[7] aurones (riccionidin type)[8] and 2,2'-spirochromenes.[9]
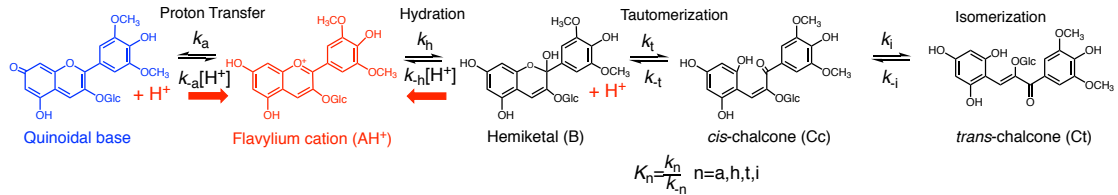


**Scheme 1**. Multistate of species of malvidin-3-glucoside in acidic to moderately acidic medium. More species are formed at higher pH values due to the deprotonation of the hydroxyl substituents.

In acidic medium, the sequence of reactions after a pH jump from a very acidic solution (generally at pH≤1) where the only species in solution is flavylium cation to higher pH values is accounted for by eq.(1) to eq.(4).

$$AH^+ + H_2O \underset{k_{-a}}{\overset{k_a}{\rightleftharpoons}} A + H_3O^+ \qquad K_a \qquad \text{proton transfer} \qquad (1)$$

$$AH^+ + 2H_2O \underset{k_{-h}}{\overset{k_h}{\rightleftharpoons}} B + H_3O^+ \qquad K_h \qquad \text{hydration} \qquad (2)$$

$$B \underset{k_{-t}}{\overset{k_t}{\rightleftharpoons}} Cc \qquad K_t \qquad \text{tautomerization} \qquad (3)$$

$$Cc \underset{k_{-i}}{\overset{k_i}{\rightleftharpoons}} Ct \qquad K_i \qquad \text{isomerization} \qquad (4)$$

In most systems, the proton transfer (acidic medium) takes place in microseconds, the hydration in minutes, the tautomerization in seconds and the isomerization in hours. This is a convenient situation for experimental study because upon addition of base to equilibrated solutions of the flavylium cation at pH≤1 (direct pH jumps), there are three distinct kinetic process that can be studied separately: i) proton transfer, a process faster than the dead time of the stopped-flow, ii) hydration followed by the faster tautomerization process, iii) the slowest isomerization step to reach the equilibrium.

A particular feature of the flavylium multistate is that eq.(1) to eq.(4) can be reduced to a single acid-base equilibrium as show in eq.(5),

$$\textbf{AH}^+ + H_2O \rightleftharpoons \textbf{CB} + H_3O^+ \qquad K_a^{'} \tag{5}$$

where

$$[\textbf{CB}] = [\textbf{A}] + [\textbf{B}] + [\textbf{Cc}] + [\textbf{Ct}] \tag{6}$$

and $K_a^{'}$ is related through eq.(7) to the equilibrium constants in eq.(1) to eq.(4). If protonable groups such as amines are attached to the flavylium core, a set of equations similar to eq.(1) to eq.(7) can be written for protonated species in equilibrium with those already described. The same applies upon deprotonation of phenol groups often present in these compounds, now involving equilibrium with monodeprotonated species.

$$K_a^{'} = K_a + K_h + K_hK_t + K_hK_tK_i \tag{7}$$

Among the several species present in flavylium multistate systems, chalcones are of particular relevance for their demonstrated biological activity and a diversity of natural and synthetic chalcones have been exploited in medicinal chemistry for drug discovery.[10] On the other hand, flavylium cations are also recognized by their role as radical scavengers, although to a less extent than the neutral hemiketal and chalcone species.[11,12] Knowledge of the mole fraction distribution of species with pH is thus crucial for flavylium-based systems because it defines the availability of each species under specific conditions.[11, 13, 14] In anthocyanins and in most related compounds, flavylium cation is the sole species at pH≤1 and the neutral species prevail for higher pH values.

The introduction of heterocycles in the chalcone 1,3-diaryl-2-propen-1-one structural core has gained attention in recent years.[15,16,17] In particular, the pyridine moiety was introduced in chalcones that have been claimed to possess anticancer activity.[18,19] In previous work, it was reported that substitution by pyridine of flavylium's phenyl B ring prevents formation of flavylium cation under acidic conditions, Scheme 2.[20] Protonation of the pyridine nitrogen for pH<4 creates a positive charge in the

pyridinechalcone that inhibits formation of the positively charged pyrylium moiety present in the flavylium structure. The multistate of pyridinechalcone is composed by all species except flavylium and has allowed studying the photochemical conversions between chalcones and hemiketal with no interference from flavylium formation.[20]
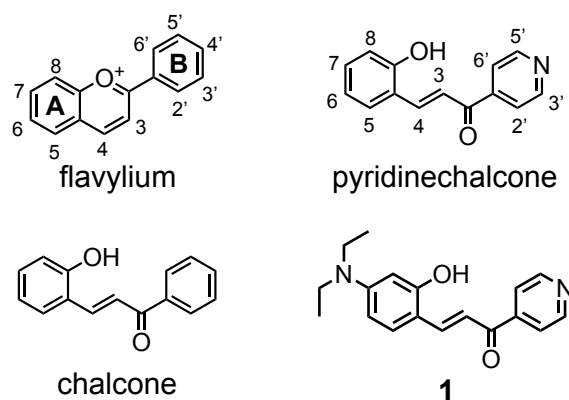


**Scheme 2.** Flavylium cation and respective chalcone, *trans*-pyridinechalcone previously reported[20] and 7-diethylamino-2-(pyridin-4-yl)-1-benzopyrylium (**1**) reported in this work.

Our challenge was to design a pyridine-based multistate system, comprising chalcones, hemiketal and flavylium, as a model system for pyridinechalcone derivatives. Introduction of an amino group in the pyridinechalcone structure could lead to a system where protonation would preferentially occur at the amine rather than at the less basic pyridine nitrogen, allowing in principle formation of the flavylium species under acidic conditions. Compound **1**, a new diethylamino derivative of pyridinechalcone, Scheme 2, was designed on the basis of this rationale. Here we present the synthesis, crystal structure and full characterization of the pH-dependent multistate of compound **1** as a model compound for pyridinechalcone derivatives.

**Results and Discussion**

Compound **1** was synthesized from condensation of 4-diethylamine-2-hydroxybenzaldehyde with 4-acetylpyridine under basic conditions. Crystals suitable for X-ray diffraction were obtained upon slow diffusion of diethyl ether over a concentrated methanolic solution of **1**.

The molecular structure of compound **1** was unambiguously established by X-ray diffraction. A Mercury diagram of the asymmetric unit is depicted in Fig. 1, the most significant bond distances and angles being given in the corresponding caption. The

dihedral angles in the caption of Fig. 1 demonstrate the quasi-planarity of this pyridinechalcone.
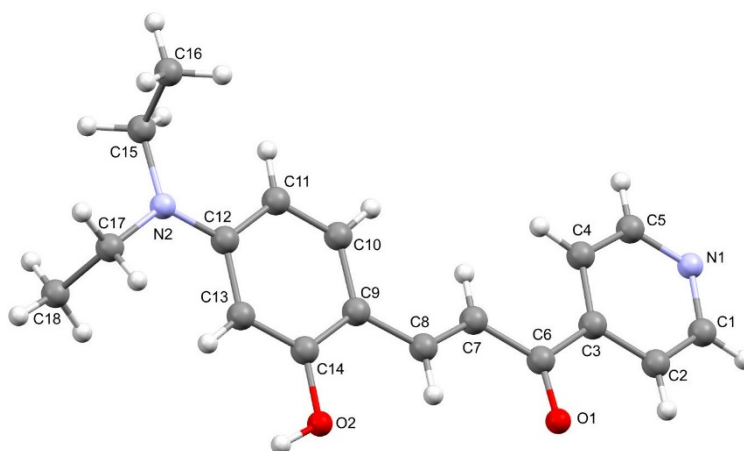


**Figure 1.** Mercury drawing of the molecular structure of compound **1**. Selected bond lengths (Å): C6−C3, 1.509(3); C7−C6, 1.439(3); C8−C7, 1.341(3); O1−C6, 1.227(3); C9−C8, 1.437(3); selected bond angles (º): C7–C8–C9, 127.8(2); C8–C7–C6 123.2(2); O1–C6–C7, 122.9(2), O1–C6–C3, 118.3(2); selected dihedral angles (º): C9–C8–C7–C6, 177.6(2); C7–C6–C3–C4, 2.4(3); C10–C9–C8–C7, -9.0(4).

Compound **1** crystallized as brown prisms in the monoclinic system, space group $P2_1/n$, with one molecule in the asymmetric unit. Its molecular structure consists of the (*E*) isomer of prop-2-en-1-one, containing as substituents pyridinyl and 4-(diethylamino)-2-hydroxyphenyl moieties. All distances and angles are within the expected values for similar compounds.[21] The supramolecular arrangement in **1** is best described as an infinite 1D-chain, being generated by intermolecular classic O–H···N hydrogen bonds, and intramolecular C–H···O assisted non-classical hydrogen bonds as presented in Fig. 2 and Table 1.
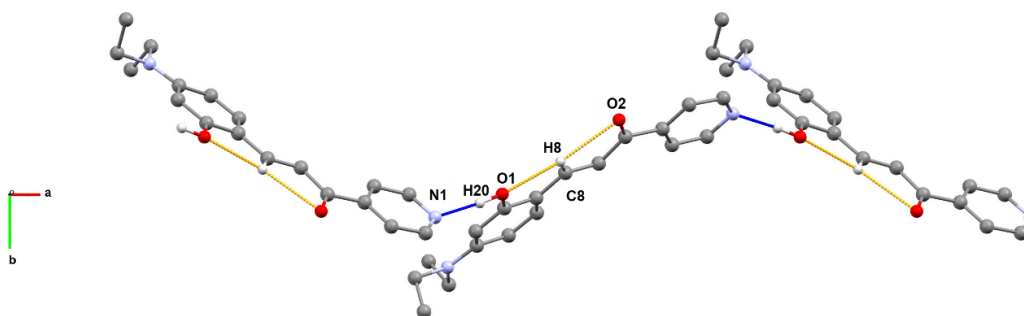
**Figure 2.** Supramolecular arrangement in compound **1**, viewed along *c*, generated by the formation of inter- and intramolecular hydrogen bonds. Donor and acceptor atoms are identified. Blue dashed lines represent the intermolecular O–H···N hydrogen bonds, and orange dashed lines the intramolecular C–H···O assisted non-classical hydrogen bonds. All hydrogen atoms, except those involved in the interactions, were omitted for clarity.

**Table 1.** List of hydrogen bonds for compound **1** [Å and °].

| D-H...A | $d$(D-H) | $d$(H...A) | $d$(D...A) | <(DHA) |
|---|---|---|---|---|
| O(1)-H(20)...N(1)[i] | 0.96 | 1.85 | 2.8143(3) | 177 |
| C(8)-H(8)...O(1) | 0.93 | 2.53 | 2.8407(3) | 100 |
| C(8)-H(8)...O(2) | 0.93 | 2.43 | 2.7890(3) | 103 |

[i] symmetry operation: $-3/2 + x$, $1/2 - y$, $-1/2 + z$

With the scope of simplifying the discussion of this complex system, the multistate of chemical species characterizing compound **1** is *a priori* presented in Scheme 3 and each step will be justified through the work with data obtained from pH jumps followed by UV-Vis. and $^{1}$H NMR as well as $^{13}$C NMR.
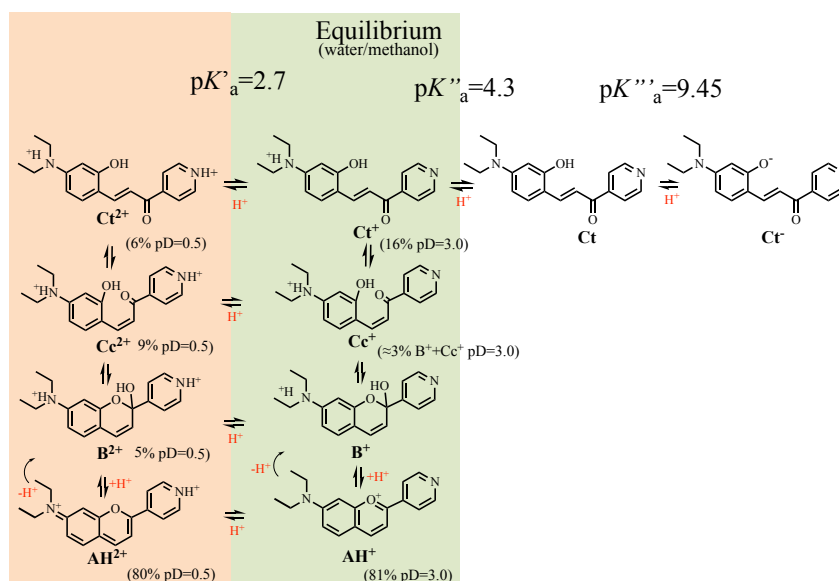
**Scheme 3**. The multistate of species observed in compound **1**.

The spectral variations of compound **1** at the equilibrium as a function of pH are shown in Fig. 3. In very acidic medium, protonated flavylium cation $AH^{2+}$ is the main species, in equilibrium with the doubly protonated species $B^{2+}$, $Cc^{2+}$ and $Ct^{2+}$, Scheme 3. Evidence for the existence of these species as well as for the positive charge in the diethylaminobenzopyrylium moiety being preferentially located in the amine nitrogen in position 7 rather than in the pyrylium oxygen is given below through ^{1}H NMR data (Fig. 10). The absorption spectrum of $AH^{2+}$ (red trace in Fig. 3A) is red-shifted in comparison to the spectrum of $AH^+$ that appears at higher pH values (blue trace in Fig. 3A). This is similar to what is observed in quinoidal bases, also red-shifted relatively to the respective flavylium cations,[13] and reflects the more extensive charge delocalization in these species; notice the structural similarity between $AH^{2+}$ in Scheme 3 and a quinoidal base like the one in Scheme 1. Under less acidic solutions (pH=3.1), the flavylium cation $AH^+$ is in equilibrium with protonated *trans*-chalcone $Ct^+$, *cis*-chalcone $Cc^+$ and hemiketal $B^+$. The next equilibrium is illustrated in Fig. 3B and reflects the existence of neutral *trans*-chalcone as the sole species around pH=6.5 (orange trace). Finally, in basic medium the deprotonated *trans*-chalcone $Ct^-$ is the only observed species, Fig. 3C. Overall fitting of the data in Figs. 3A-3C defines three observed $pK_a$ values, $pK'_a$=2.7, $pK''_a$=4.3, $pK'''_a$=9.5 (Fig. 3D) that correspond to the equilibria between deprotonated, monoprotonated, neutral and deprotonated species. These results have been corroborated by ^{1}H NMR, see below (Fig. 9).
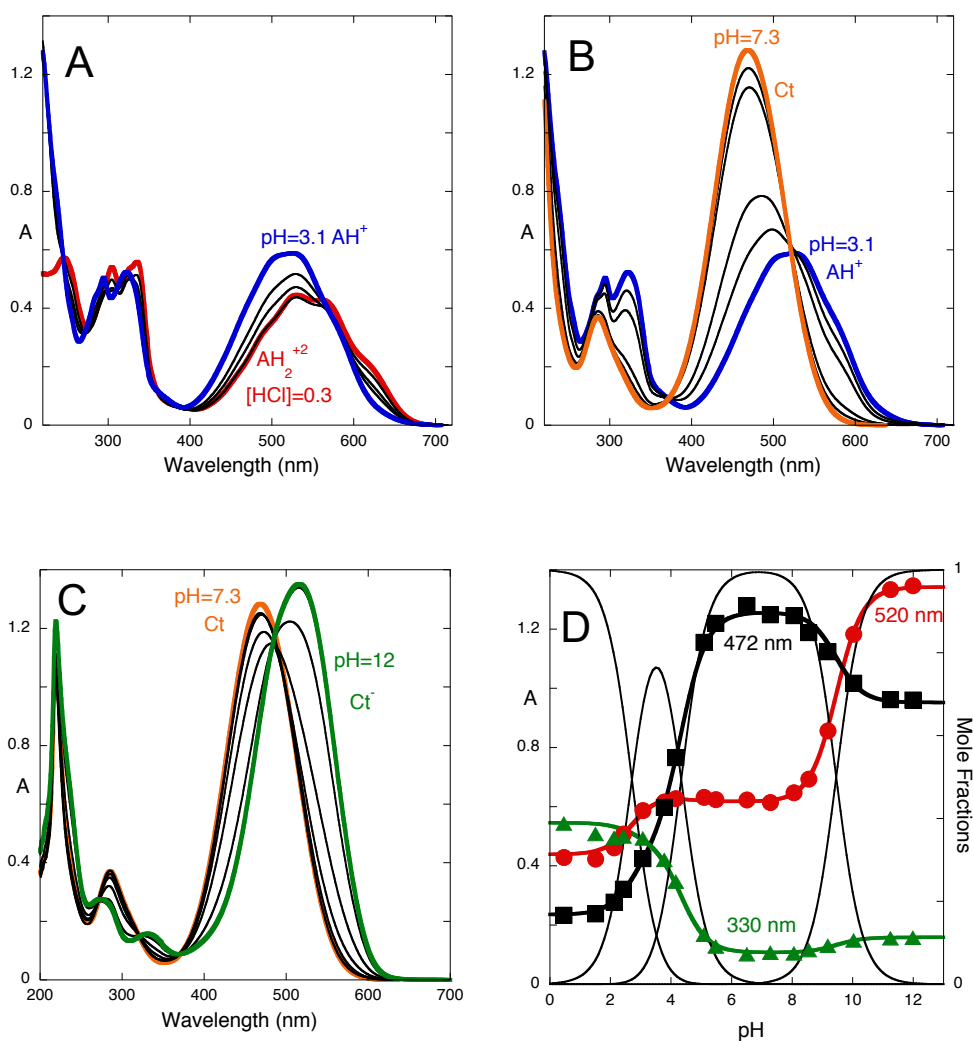
**Figure 3**. Absorption spectra of equilibrated solutions of compound **1** after direct and reverse pH jumps from pH=6.5 (neutral *trans*-chalcone, $1.1 \times 10^{-4}$ M water:methanol 1:1 (v/v)) to the following pH changes: **(A)** ~0.5 (HCl 0.3 M)<pH< 3.1; **(B)** 3.1<pH<7.3; (C) 7.3<pH<12. **(D)** Simultaneous fitting of absorbance data at 330, 472 and 520 nm leads to the following global acidity constants: p$K'_a$=2.7, p$K''_a$=4.3, p$K'''_a$=9.5, with the corresponding mole fraction distribution of species.

A series of stopped-flow experiments were carried out to follow the kinetics of the system after specific pH jumps. The first series consisted in jumps from a solution at pH=6.4 containing only **Ct** to more acidic pH values. In Figure 4A, the spectral variations occurring after a pH jump to pH=6, where doubly protonated species prevail, show the existence of two kinetic processes. Protonation of **Ct** occurs during the mixing time to form **Ct²⁺**. The first kinetic step is finished after 5 s and should correspond to the disappearance of **Ct²⁺** to give **Cc²⁺**. The slower process is characterized by the raising of a structured absorption band centered at 525 nm, indicating the formation of protonated flavylium cation, **AH²⁺**. The rate constants of

the two kinetic steps $k_1$=0.5 s$^{-1}$ and $k_2$=0.003 s$^{-1}$ were obtained by fitting the absorption at 365 nm, Fig. 4A. The kinetics of the same pH jump was also monitored by a common spectrophotometer, Fig. 4B. The spectral variations show the formation of more **AH$^{2+}$** species with a rate constant of 0.003 s$^{-1}$, equal to the slowest step in Fig. 4A.
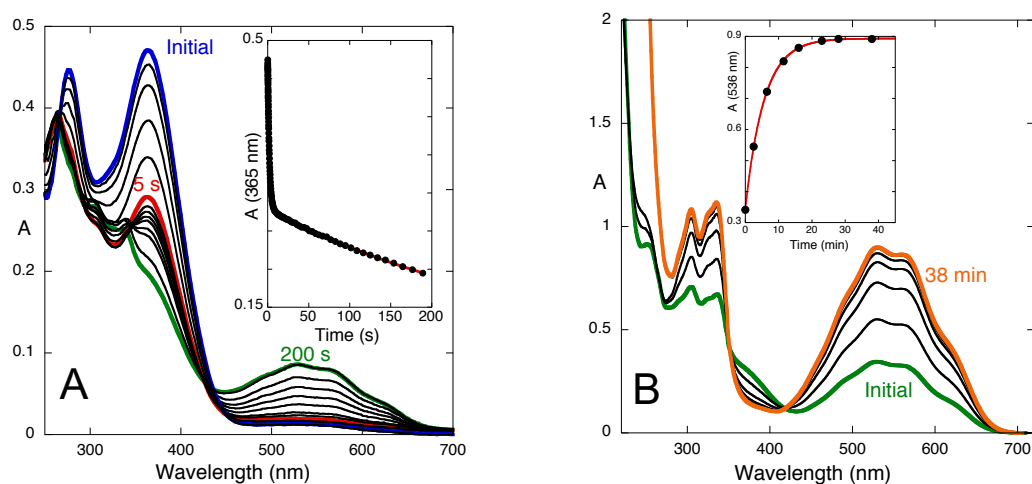


**Figure 4**. Spectral variations upon a pH jump from a solution of compound **1** equilibrated at pH=6.4 (neutral *trans*-chalcone, water:methanol 1:1 (v/v)) to pH=0.6, **(A)** followed by stopped-flow, [**1**]=9.0x10$^{-5}$ M; inset: fitting was achieved with a bi-exponential law with rate constants 0.5 s$^{-1}$ and 0.003 s$^{-1}$; **(B)** followed by a common spectrophotometer, [**1**]=1.8x10$^{-4}$ M; inset: fitting was achieved with a mono-exponential law with rate constant 0.003 s$^{-1}$.

Considering the behavior of anthocyanins and related compounds, the slowest process with rate constant 0.003 s$^{-1}$ could be explained by a fast tautomerization followed by a slower hydration that would kinetically control this step. However, there is another possible explanation: the kinetic control by automerization followed by a faster hydration reaction. pH jumps from solutions equilibrated at lower pH values to pH=6.4 (**Ct**) together with NMR data reported below show that this is the case in this compound.

9
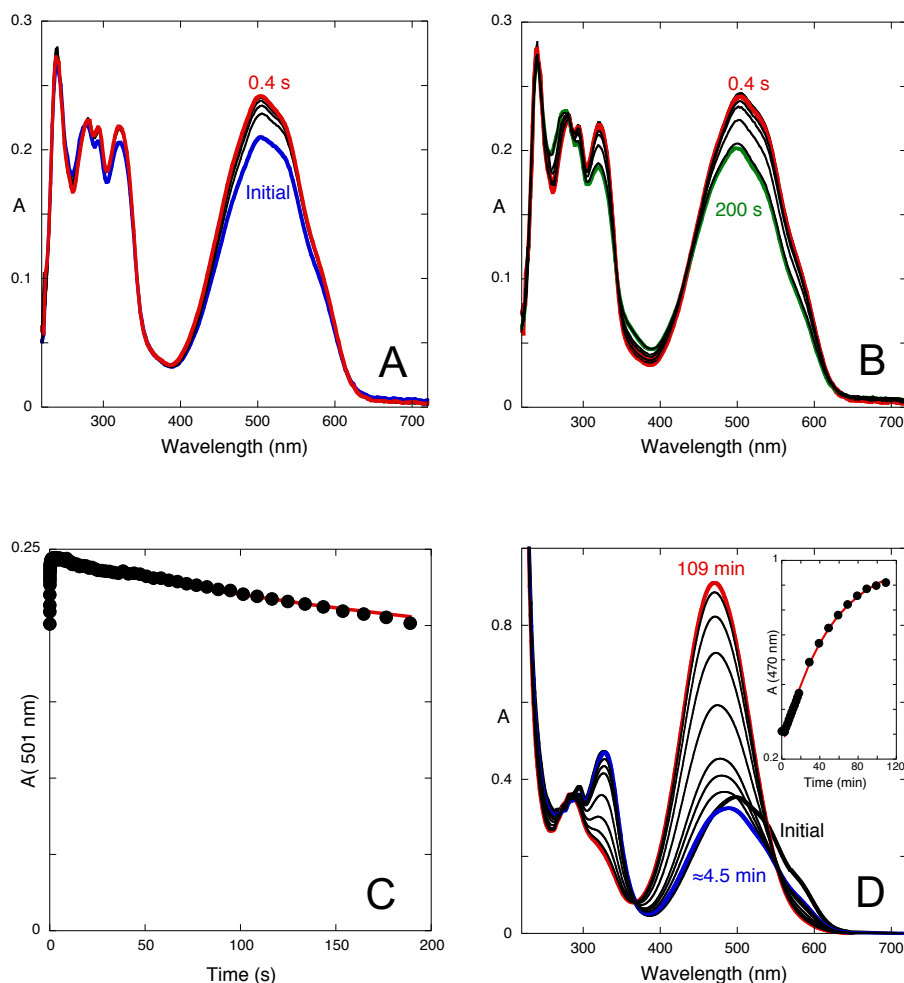
**Figure 5**. Spectral variations upon a pH jump from a solution of compound 1 equilibrated at pH=6.4 (9.0x10⁻⁵ M, water:methanol 1:1) followed by stopped-flow: **(A)** during the first 0.4 seconds; **(B)** between 0.4 s and 200 s; **(C)** absorbance at 501 nm fitted with a bi-exponential law with rate constants 9.9 s⁻¹ and 0.004 s⁻¹; **(D)** the same pH jump followed by a common spectrophotometer, [**1**]=1.8x10⁻⁴ M; fitting was achieved with a mono-exponential law with $k_{obs}$=3.4x10⁻⁴ s⁻¹.

pH jumps from solutions equilibrated at pH=0.6 to pH=6.4 are shown in Fig. 5. In this case, three kinetic steps with rate constants 9.9 s⁻¹, 0.004 s⁻¹ and 3.4x10⁻⁴ s⁻¹ were observed. Moreover, the absorbance in the visible increases in the first step, decreases in the second and increases again in the third. Immediately after the pH jump, all species that were present at pH=0.6 become deprotonated, "frozen" in their mole fractions at the initial pH of the pH jump. Consequently, the initial spectra at pH=6.4 correspond to the absorptions of **Ct**, **Cc**, **B** and **AH⁺** in the mole fractions of **Ct**, **Cc²⁺**, **B²⁺** and **AH²⁺** initially present at pH=0.6. Considering that in solutions equilibrated at pH=6.4 **Ct** is the sole species, all the other should evolve to **Ct**. The peculiar behavior is the decreasing of the absorbance in the visible in the second step. Sequential formation of

**Ct** from conversion of **Cc**, then **B** (via **Cc**) and **AH⁺** (via **B** and **Cc**) is not observed. Such a process would give rise to a stepwise increase in **Ct** absorbance. Our interpretation is that the first kinetic step is the conversion of **Cc** into **Ct**. The next kinetic step is the hydration of **AH⁺** to give **B**, with the corresponding decrease of the absorbance in the visible. The slowest kinetic step is assigned to the conversion of **B** into **Ct** (via **Cc**), affirming the tautomerization reaction as rate-limiting step.
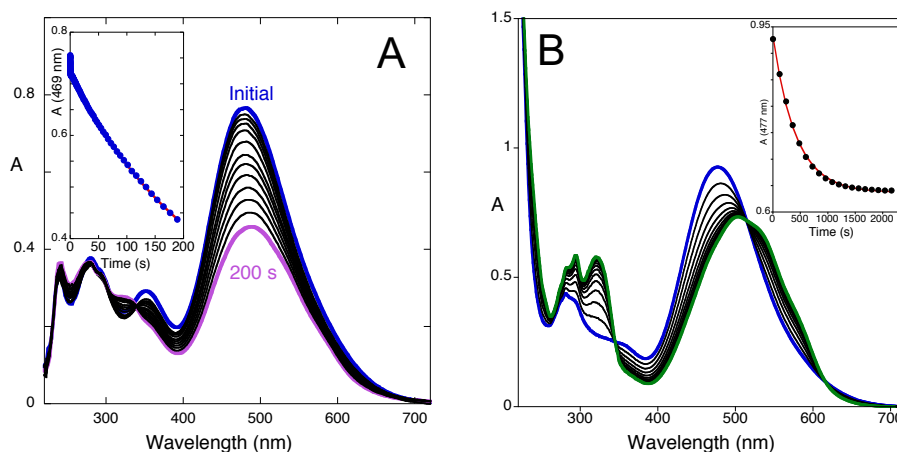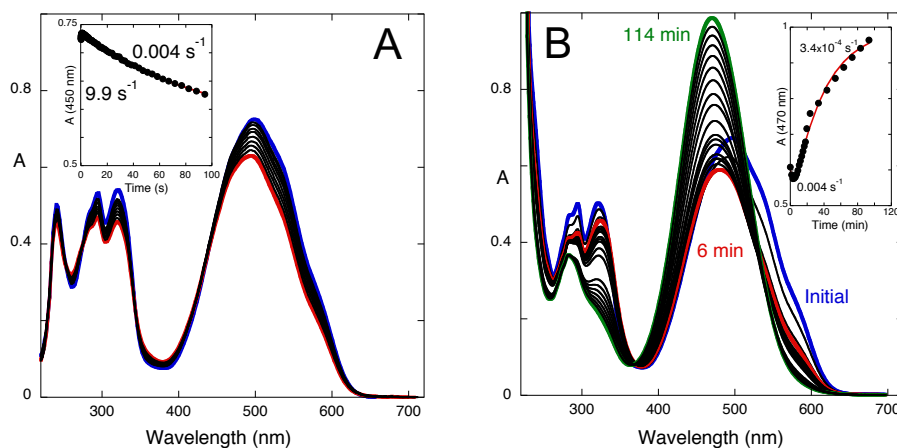


**Figure 6.** Spectral variations after a pH jump from a solution of compound **1** equilibrated at pH=6.4 ($9.0 \times 10^{-5}$ M, water:methanol 1:1 (v/v)) to pH=3.4 followed by: **(A)** stopped-flow; inset: two processes were observed with rate constants 0.9 s$^{-1}$ (small amplitude) and 0.003 s$^{-1}$; **(B)** a common spectrophotometer, [**1**]=$1.8 \times 10^{-4}$ M; inset: fitting with a mono-exponential law with rate constant 0.003 s$^{-1}$.

A pH jump from pH=6.4 to pH=3.4, where mono-protonated species are present, was performed, Fig. 6. The results are qualitatively similar to those presented in Fig. 4 and the respective rate constants are 0.9 s$^{-1}$ and 0.003 s$^{-1}$. However, the amplitude of the first process, the one that corresponds to the formation of **Cc⁺** from **Ct⁺**, is very small indicating that the equilibrium between these two species is shifted to the *trans* isomer. The last step corresponds to the formation of flavylium cation via **Cc⁺** and **B**, which was confirmed by the next set of pH jumps.

A set of pH jumps from equilibrated solutions of the compound at pH=3.4 to pH=6.4 have been carried out. The pH jump monitored by stopped-flow shows the existence of two processes with rate constants 9.9 s$^{-1}$ and 0.004 s$^{-1}$, Fig. 7A. The same experiment followed by a common spectrophotometer shows a single process with rate constant $3.4 \times 10^{-4}$ s$^{-1}$ (Fig. 7B) that is identical to the slowest one observed in the previous set of pH jumps (Fig. 5D). However, the amplitude of the traces is different. The amplitude

of the first process in the pH jump from 0.6 to 6.4 (Fig. 5C) is higher than in the pH jump 3.4 to 6.4 (Fig. 7A). This means that there is more **Cc²⁺** in the equilibrium at pH=0.6 than **Cc⁺** at pH=3.4, as corroborated by ¹H NMR (see below, Fig. 9).



**Figure 7**. Spectral variations after a pH jump from an equilibrated solution of compound **1** at pH=3.4 (9.0x10⁻⁵ M, water:methanol 1:1 (v/v)) to pH=6.4; (**A**) the two first kinetic steps, followed by stopped-flow; (**B**) the slowest process, followed by a common spectrophotometer.

Scheme 4 describes conversion rates and composition of the multistate at pH values 0.6, 3.4 and 6.4, summarizing the above results from direct and reverse pH jumps.
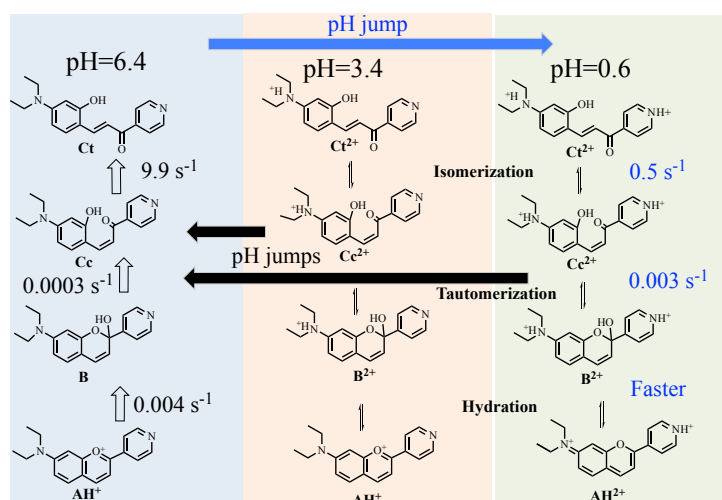


**Scheme 4**. Summary of the multistate composition of compound **1** and conversion rates at pH 0.6, 3.4 and 6.4.

Extending the pH jumps from pH=6.4 to other lower pH values leads to results similar to those in Fig. 4 and Fig. 6. The two rate constants resulting from the respective fittings

are plotted in Fig. 8. The faster process, assigned to the *cis-trans* isomerization, decreases in the order **Ct** $\approx$ **Ct⁺** < **Ct²⁺**. Regarding the slower process, assigned to the tautomerization reaction, the mono and diprotonated species of **B** and **Cc** tautomerize with the same rate constant within the experimental error. However, the rate of tautomerization process for the neutral species, assessed from pH jumps to 6.4 from lower pH values is significantly slower (Fig. 8B).

Determination of the acidity constants of the *trans*-chalcones protonated at the amine and pyridine nitrogens was carried out by stopped-flow to obtain $pK_{Ct2+/Ct+}$=2.2 and $pK_{Ct+/Ct}$=3.8 (Supplementary Information (SI), Fig. S1). The acidity constant for phenol deprotonation in **Ct**, $pK_{Ct/Ct-}$=9.5, is obtained from Fig. 3c.
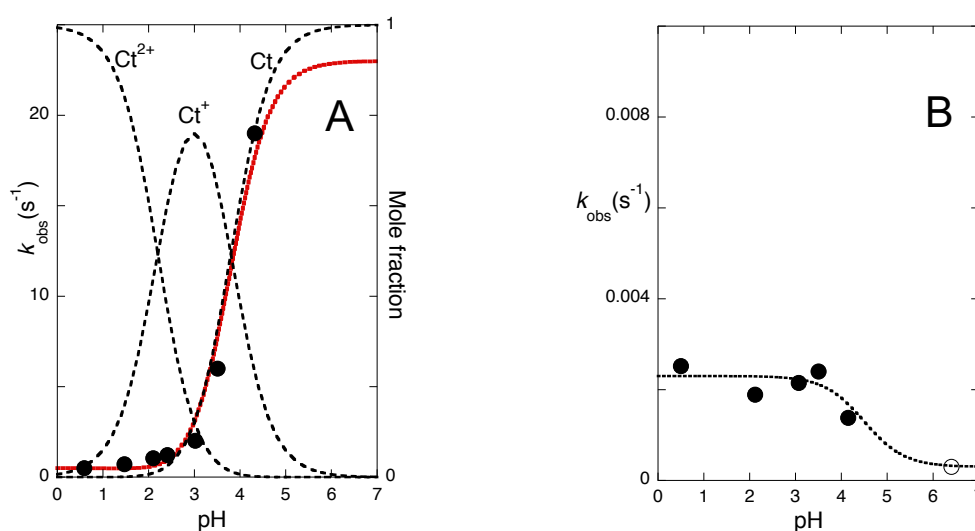


**Figure 8.** (A) pH dependence of the rate constants of the faster process after pH jumps from pH=6.4 to lower pH values. Fitting was achieved with isomerization constants of 0.5 s⁻¹, 0.3 s⁻¹ and 23 s⁻¹ for **Ct²⁺**, **Ct⁺** and **Ct**, respectively, taking into account the $pK_a$ values $pK_{Ct2+/Ct+}$=2.2 and $pK_{Ct+/Ct}$=3.8. The error associated with these rate constants is ~30%. (B) Rate constants of the slower process as a function of pH; (●) pH jump 6.4 to lower pH jumps; (○) pH jumps from pH=3.4 (or 0.6) to 6.4.

*¹H NMR*

Fig. 9 shows the ¹H NMR spectra of equilibrated solutions at three representative pD values, the lower (pD=0.5) corresponding to di-protonated species, the middle to mono-protonated species and the higher to neutral species.
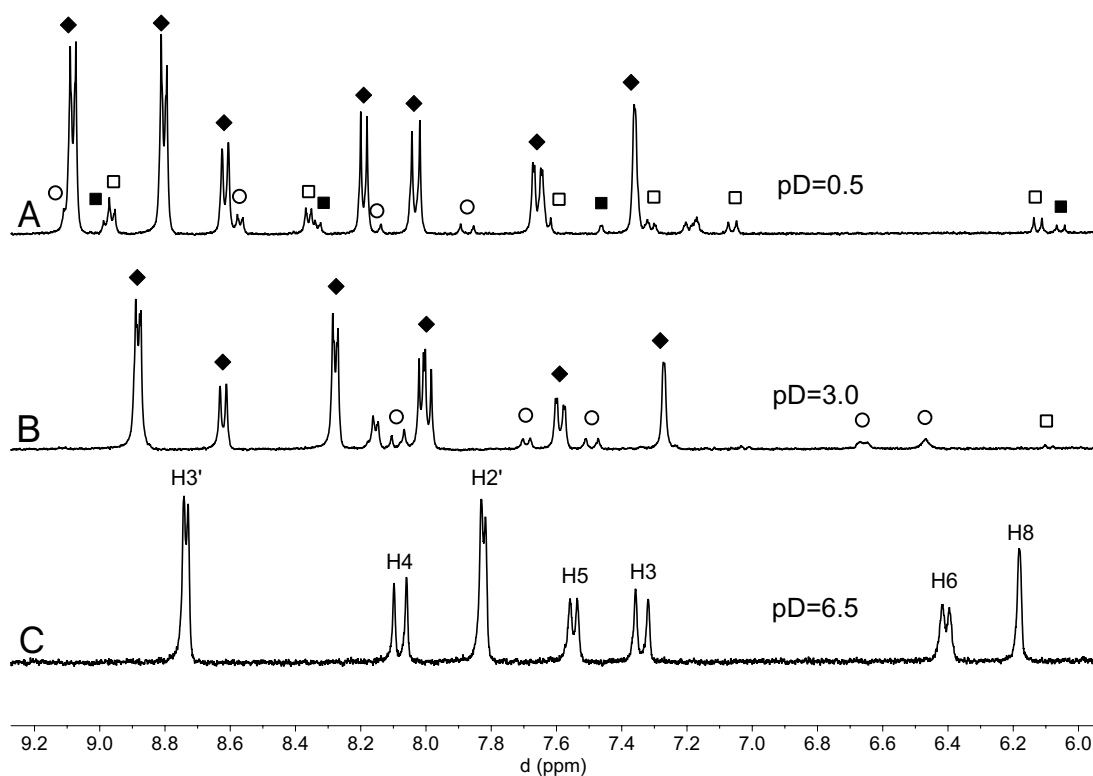
**Figure 9**. Aromatic part of the ¹H NMR spectra of $1.7 \times 10^{-3}$M solutions of compound **1** (CD₃OD/D₂O 1:1 (v/v), 400 MHz) equilibrated in the dark at: **(A)** pD=0.5; 80% **AH²⁺** (◆); 6% **Ct²⁺** (◯); 9% **Cc²⁺** ( ); 5% **B²⁺** (■); **(B)** pD=3; 81% **AH⁺** (◆), 16% **Ct⁺** (◯), ~ 3% **B⁺ + Cc⁺** ( ); **(C))** pD=6.5; the system does not evolve at this pH (100% **Ct**).

At pD=6.4 the only species in solution is the *trans*-chalcone form of compound **1**, as revealed by spectrum c) in Fig. 9 (see SI for full assignment of **Ct**, **AH⁺** and **AH²⁺**, Tables S1, S2 and S3, respectively). At pD=3, the presence of **Ct⁺** (16%) is indicated by the large coupling constant (15.3 Hz) of protons 3 and 4 in equilibrium with a major species, assigned to the flavylium cation **AH⁺**. The intermediate species **Cc⁺** and **B⁺** account for ca. 3%. At the most acidic pD value (0.5), the multistate system is again dominated by a flavylium species, **AH²⁺** (80%), in equilibrium with di-protonated species **Ct²⁺**, **Cc²⁺** and **B²⁺**. The **AH²⁺** species is protonated at the pyridine nitrogen as revealed by the low field chemical shift of the pyridine ring protons (Fig. 9A). Moreover, the multiplicity of the methylene and methyl groups of the diethylamino moiety observed in the ¹H NMR spectrum of **AH²⁺**, Fig. 10, show that the two ethyl groups are magnetically non-equivalent. This indicates that the positive charge in the benzopyrylium moiety, pushed by the positive charge of the pyridinium group, is mainly located in the amine nitrogen and not in the pyrylium oxygen, Fig. 10. Such

signal splitting of the diethylamino peaks is not so evident for the $\mathbf{AH^+}$ species (pD=3), suggesting that the positive charge in this species is much more localized in the pyrylium oxygen. This implies that formation of $\mathbf{AH^+}$ from $\mathbf{B^+}$ involves a prototropic rearrangement where the ammonium proton is transferred to the hemiketal hydroxyl group in $\mathbf{B^+}$ followed by dehydration.
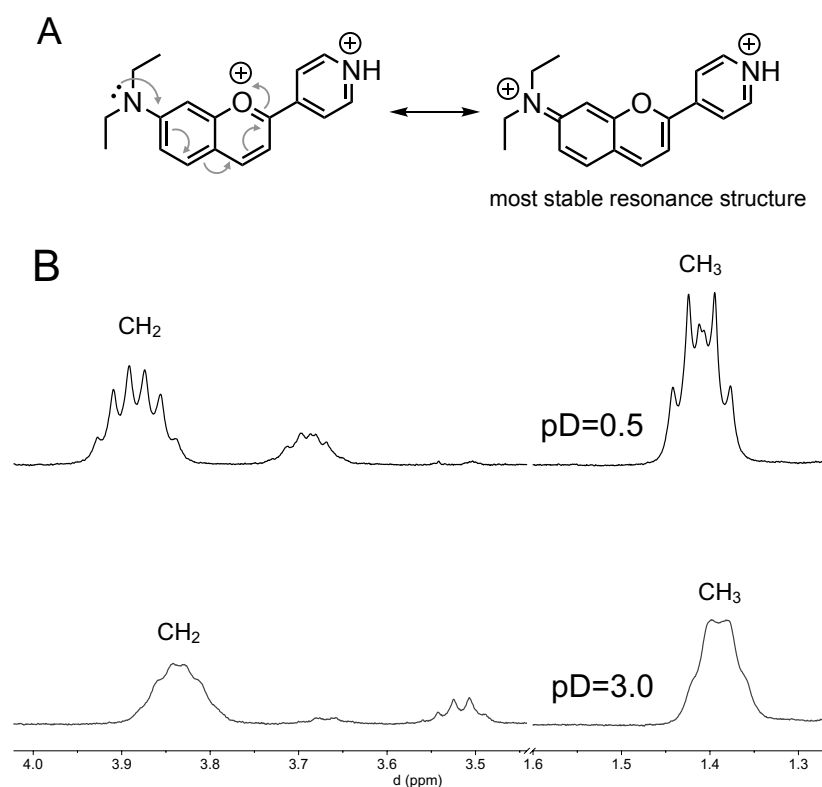


**Figure 10. (A)** Positive charge delocalization in the benzopyrylium moiety of $\mathbf{AH^{2+}}$ species of compound **1**; **(B)** detail of the $^1$H NMR spectra covering the diethylamino peaks.

For each pH jump, $^1$H NMR spectra were acquired over time until the equilibrium was established (see SI, Fig. S6 and S11). Integration of selected peaks allows to plot kinetic traces for each species, as shown in Fig. 11.
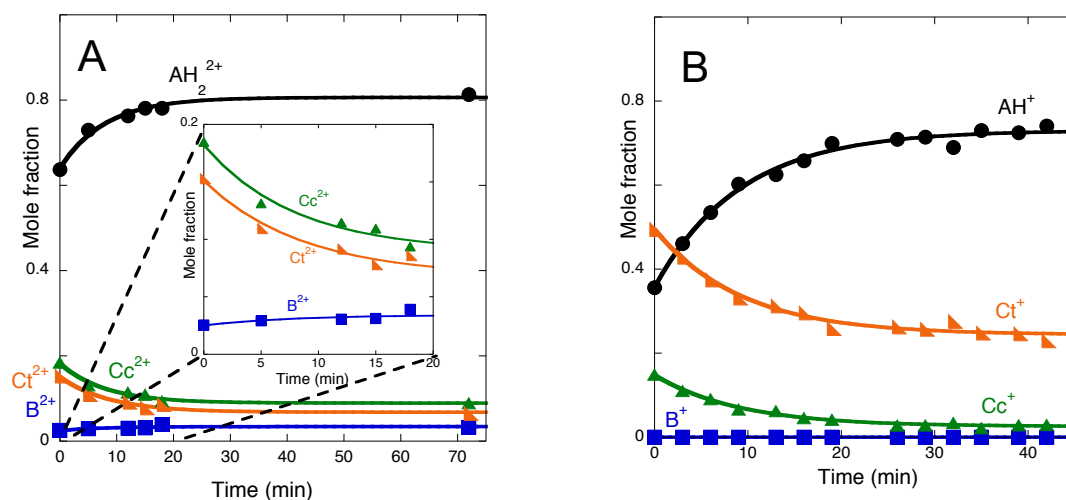
**Figure 11**. Time evolution of the species mole fraction distribution during the slowest kinetic step after a pH jump from pD=6.4 (100 % **Ct**) to: (**A**) pD=0.5; (**B**) pD=3.0; data obtained by integration of the ${}^1$H NMR peaks ([**1**]=1.7x10${}^{-3}$M, CD${}_3$OD/D${}_2$O 1:1 (v/v)).

The ${}^1$H NMR shown in Fig. 11 corroborates the interpretation given from the UV-vis data above reported. Because the first ${}^1$H NMR spectrum is finished 10-15 min after the pH jump and the first kinetic step takes only a few seconds (see Fig. 4A and 6A), the kinetic traces in Fig. 11 describe the slowest process, after the initial isomerization of the chalcones has taken place. Indeed, at pD=0.5, these two species remain in equilibrium from the beginning with a ratio [**Ct${}^{2+}$**]/[**Cc${}^{2+}$**]=0.7=$K_i^{2+}$. Similarly, **AH${}^{2+}$** and **B${}^{2+}$** evolve simultaneously and maintain a constant ratio [**B${}^{2+}$**]/[**AH${}^{2+}$**]=0.05. On the contrary, the ratio [**Cc${}^{2+}$**]/[**B${}^{2+}$**] decreases until the equilibrium is reached with [**Cc${}^{2+}$**]/[**B${}^{2+}$**]=1.8=$K_t^{2+}$. These data lead the tautomerization process as the rate-limiting step as anticipated above from UV-Vis absorption data. It is worth of note that in this case, the rate constants $k_t^{2+}$=1.9x10${}^{-3}$ s${}^{-1}$ and $k_{-t}^{2+}$=1.1x10${}^{-3}$ s${}^{-1}$ can be calculated from $k_t^{2+}+k_{-t}^{2+}$=0.003 s${}^{-1}$ and $K_t^{2+}$=1.8; similarly, $k_i^{2+}$=0.21 s${}^{-1}$ and $k_{-i}^{2+}$=0.29 s${}^{-1}$ can be calculated from $k_i^{2+}+k_{-i}^{2+}$=0.5 s${}^{-1}$ and $K_i^{2+}$=0.7.

**Conclusions**

Flavylium cations in aqueous solutions give rise to multistate chemical reaction networks comprising several species with known biological activity. Introduction of heterocycles in the flavylium core is an active research field in prospecting new bioactive structures. When the phenyl ring in position 2 is substituted by a pyridine, no flavylium cation is observed due to protonation of the pyridine. Introduction of a diethylamino substituent in position 7 of pyridinechalcone, which is easily protonated

when compared to pyridine, permits the appearance of a new family of pyridineflavylium derivatives. In this particular system, not only pyridineflavylium is formed between pH 2 and 4 but a double positively charged species, protonated in the amino and the pyridine moieties, is also formed for pH<1. Detailed NMR characterization of the these new flavylium species shows large delocalization of the pyrylium positive charge over the diethylamino moiety already at the monopositively charged flavylium opening perspectives for interaction of these species with DNA. Full characterization of the kinetics and thermodynamics of this multistate system shows that, differently from anthocyanins and related compound, the ring-opening closure reaction between hemiketal and *cis*-chalcone, becomes much slower than cis-trans chalcone isomerization. The present system opens perspectives for the design and biological activity study of pyridinechalcone derivatives.

**Experimental part**

*Materials and Methods.* All reagents and solvents were purchased from Sigma-Aldrich and were of analytical grade ($\geq 97\%$), including those used in the preparatrion of the buffer solutions. The NMR spectra at 300.0 K were obtained using a Bruker AMX400 operating at 400.13 ($^1$H) and 100 MHz ($^{13}$C). NMR assignments have been carried out on the basis of 1D ($^1$H, $^{13}$C) and 2D (COSY, HSQC and HMBC) NMR spectra. Elemental analyses were performed using a Thermofinnigan Flash EA 1112 Series instrument with an error of ±0.4%. Mass spectra were obtained on an Orbitrap XLTM LTL (ESI-MS) controlled by LTQ Tune Plus 2.5.5 and Xcalibur 2.1.0.

*Synthesis and characterization of (E)-3-(4-(diethylamino)-2-hydroxyphenyl)-1-(pyridin-4-yl)prop-2-en-1-one (**1**)*

A solution of 0.55 mL of 4-acetylpyridine (5 mmol) and 0.984 g of 4-diethylaminosalicylaldehyde (5.1 mmol) in 7.5 mL of ethanol was degassed. Then, 0.45 mL of an aqueous solution of KOH (1 g / mL) was added dropwise at room temperature, under nitrogen. The reaction mixture was degassed again and stirred at room temperature overnight under inert atmosphere. The solution was neutralized and concentrated under reduced pressure to give a crude residue, which was first purified by flash column chromatography (DCM:EtOAc, 8:2, v/v) and then recrystallized in MeOH:Et$_2$O (2:1) to give brown-purple crystals (0.100 g, 14%). $^1$H NMR (400 MHz,

Acetone-d6) δ 9.02 (s, 1H, OH), 8.80 (d, 2H, H3 '+ H5'), 8.18 (d, J = 16 Hz, 1H, H4), 7.86 (D, J = 8.9 Hz, 1H, H5), 7.53 (d, J = 16 Hz, 1H, H3), 6.37 (dd, J = 8.9, 2.5 Hz, 1H , 1.44 (t, J = 7.0 Hz, 6H, 2 CH 3); 13 C NMR (101 MHz, Acetone-d 6) ) δ 188.3 (C2), 157.6 (C10), 151.7 (C9), 150.5 (C3 '+ C5'), 145.7 (C1'), 142.6 (C4), 131.1 (C5), 121.3 (C2' + C6 ') , 114.4 (C3), 110.0 (C7), 104.8 (C6), 97.5 (C8), 44.2 (2 $x$ CH$_2$), 12.0 (2 $x$ CH$_3$). MS (ESI-MS, positive mode): m/z 297.1603 [M+H]$^+$; calculated for [C$_{18}$H$_{21}$N$_2$O$_2$]$^+$ 297.1598. EA calculated for C$_{18}$H$_{20}$N$_2$O$_2$: %C 72.95; %H 6.80; %N 9.45; Found: %C 72.97, %H 6.49, % N 9.52.

*Single-crystal X-ray diffraction.* Crystals suitable for single-crystal X-ray analysis of compound **1** were selected and covered with Fomblin (polyfluoro ether oil) and mounted on a nylon loop. The data was collected at room temperature on a Bruker D8 Venture diffractometer equipped with a Photon 100 detector, using graphite monochromated Mo-Kα radiation (λ=0.71073 Å). The data was processed using the APEX2 suite software package, which includes integration and scaling (SAINT), absorption corrections (SADABS) and space group determination (XPREP). Structure solution and refinement were done using direct methods with the programs SHELXT 2014/5 and SHELXL (version 2018/3)[22],[23] inbuilt in APEX and WinGX-Version 2018.3[24] software packages. All non-hydrogen atoms were refined anisotropically. Except for the OH, all hydrogen atoms were inserted in idealized positions, and allowed to refine riding on the parent carbon or oxygen atom with C–H distances of 0.93 Å, 0.96 Å, and 0.97 Å, for aromatic, methyl, and methylene H atoms, respectively, and O–H distance of 0.82 Å. The molecular diagrams were drawn with Mercury[25] included in the software package. Crystal data for compound **1**: C$_{18}$H$_{20}$N$_2$O$_2$, FW = 296.36, monoclinic, space group $P2_1/n$ (no.14), D$c$ = 1.244 g cm$^{-3}$, Z = 4, a = 7.0060(6), b = 18.2400(17), c = 12.5016(11) Å, α = 90, β = 97.953(4), γ = 90 °, V = 1582.2(2) Å$^3$, T = 293(2) K, Bruker APEX-II CCD diffractometer with Photon 100 area detector, λ (MoK$_\alpha$) = 0.71073 Å, μ = 2.484 mm$^{-1}$. Of 31778 reflections measured, 2992 were unique. Refinement on $F^2$ concluded with the values $R_1$ = 0.0668 and $wR_2$ = 0.1542 for 204 parameters and 1795 data with I > 2σI. The data was deposited in CCDC under the deposit number 1920050.

*Thermodynamic and kinetic studies.* The pH jumps were carried out by adding a stock solution of *trans*-chalcone in MeOH (1.5 mL) to a 3 mL quartz cuvette containing 1.5 mL of universal buffer of Theorell and Stenhagen (1.5 mL)[26] at the desired final pH. The final pH of the solutions was measured in a Crison basic 20 + pH meter. Spectroscopic measurements were performed using Mili-Q water and methanol HPLC grade, with a constant temperature of 20±1 °C, with a Varian-Cary 100 Bio or Varian-Cary 5000 spectrophotometers. The stopped-flow experiments were conducted in an Applied Photophysics SX20 stopped-flow spectrometer provided with a PDA.1/UV photodiode array detector.

## Conflicts of interest

There are no conflicts of interest to declare.

## References

[1] P. Furtado, P. Figueiredo, H. Chaves das Neves and F. Pina, Photochemical and thermal degradation of anthocyanidins, *J. Photochem. Photobiol., A*, 1993, **75**, 113−118.

[2] L. Cabrita, V. Petrov and F. Pina, On the thermal degradation of anthocyanidins: cyanidin, *RSC Adv.*, 2014, **4**, 18939−18944.

[3] L. Cruz, V. Petrov, N. Teixeira, N. Mateus, F. Pina and V. de Freitas, Establishment of the chemical equilibria of different types of pyranoanthocyanins in aqueous solutions: evidence for the formation of aggregation in pyranomalvidin-3-O-coumaroylglucoside-(+)-catechin, *J. Phys. Chem. B*, 2010, **114**, 13232-13240.

[4] J. G. Sweeny and G. A. Iacobucci, Effect of Substitution on the Stability of 3-Deoxyanthocyanidins in Aqueous Solutions, *J. Agric. Food Chem.*, 1983, **31**, 531−533.

[5] M. J. Melo, S. Moura, A. Roque, M. Maestri and F. Pina, Photochemistry of luteolinidin: "Write-lock-read-unlock-erase" with a natural compound, *J. Photochem. Photobiol., A.*, 2000, **135**, 33−39.

[6] R. Gavara, V. Petrov and F. Pina, Characterization of the 4'-hydroxynaphthoflavylium network of chemical reactions, *Photochem. Photobiol. Sci.*, 2010, **9**, 298-303.

[7] R. Gomes, A. M. Diniz, A. Jesus, A. J. Parola and F. Pina, The synthesis and reaction network of 2-styryl-1-benzopyrylium salts: An unexploited class of potential colorants, *Dyes Pigm.*, 2009, **81**, 69−79.

[8] A. Alejo-Armijo, A. J. Parola and F. Pina, pH-Dependent Multistate System Generated by a Synthetic Furanoflavylium Compound: An Ancestor of the Anthocyanin Multistate of Chemical Species, ACS Omega, 2019, **4**, 4091–4100.

[9] A. Alejo-Armijo, L. Corici, L. Cseh, D. Aparaschivei, A. Moro, A. J. Parola, J. C. Lima and F. Pina, Achieving Complexity at the Bottom. 2,6-Bis(arylidene)cyclohexanones and Anthocyanins: The Same General Multistate of Species, *ACS Omega*, 2018, **3**, 17853-17862.

[10] C. Zuhang, W. Zhang, C. Sheng, C. Xing and Z. Miao, Chalcone: A privileged structure in medicinal chemistry, *Chem. Rev.*, 2017, **117**, 7762-7810.

[11] O. Dangles and J.-A. Fenger, The Chemical Reactivity of Anthocyanins and Its Consequences in Food Science and Nutrition, *Molecules*, 2018, **23**, 1970.

[12] A. F. Faria, M. C. Marques and A. Z. Mercadante, Identification of bioactive compounds from jambolão (Syzygium cumini) and antioxidant capacity evaluation in different pH conditions, *Food Chem.*, 2011, **126**, 1571–1578.

[13] F. Pina, M. J. Melo, C. A. T. Laia, A. J. Parola and J. C. Lima, Chemistry and Applications of Flavylium Compounds: a Handful of Colours, *Chem. Soc. Rev.*, 2012, **41**, 869−908.

[14] K. Vidot, N. Achir, C. Mertz, A. Sinela, N. Rawat, A. Prades, O. Dangles, H. Fulcrand and M. Dornier, Effect of Temperature on Acidity and Hydration Equilibrium Constants of Delphinidin-3-O- and Cyanidin-3-O-sambubioside Calculated from Uni- and Multiwavelength Spectroscopic Data, *J. Agric. Food Chem.*, 2016, **64**, 4139−4145.

[15] G. Prakash, M. Boopathy, R. Selvam, S. Johnsanthosh Kumar and K. Subramanian, The effect of anthracene-based chalcone derivatives in the resazurin dye reduction assay mechanisms for the investigation of Gram-positive and Gram-negative bacterial and fungal infection, *New J. Chem.*, 2018, **42**, 1037-1045.

[16] H. Kumar, A. Chattopadhyay, R. Prasath, V. Devaraji, R. Joshi, P. Bhavana, P. Saini and S. K. Ghosh, Design, Synthesis, Physicochemical Studies, Solvation, and DNA Damage of Quinoline-Appended Chalcone Derivative: Comprehensive Spectroscopic Approach toward Drug Discovery, *J. Phys. Chem. B*, 2014, **118**, 7257-7266.

[17] S. I. Habib and P. A. Kulkarni, Synthesis and antimicrobial activity of some new chalcones of pyridine/pyrrole carboxaldehyde, *Pharm. Lett.*, 2013, **5**,101-104.

[18] M. Mojarrad, R. Soltani and A. Aliabadi, Pyridine based chalcones: Synthesis and evaluation of antioxidante activity of 1-phenyl-3-(pyridin-2-yl)prop-2-en-1-one derivatives, *Jundishapur J. Nat. Pharm. Prod.*, 2013, **8**, 125-130.

[19] S. D. Durgapal, R. Soni, S. Umar, B. Suresh and S. S. Soman, 3-Aminomethyl pyridine chalcone derivatives: Design, synthesis DNA binding and cytotoxic studies, *Chem. Biol. Drug Design*, 2018, **92**, 1279-1287.

[20] Y. Leydet, A. J. Parola and F. Pina, Hydroxypyridinechromene and Pyridinechalcone: Two Coupled Photochromic System. *Chem. Eur. J.*, 2010, **16**, 545−555.

[21] F. H. Allen, The Cambridge Structural Database: a quarter of a million crystal structures and rising, *Acta Crystallogr., Sect. B: Struct. Sci.*, 2002, **58**, 380-388.

[22] G. M. Sheldrick, Crystal Structure Refinement with SHELXL, *Acta Crystallogr., Sect. C: Struct. Chem.*, 2015, **71**, 3-8.

[23] C. B. Hübschle, G. M. Sheldrick and B. Dittrich, ShelXle: a Qt graphical user interface for SHELXL, *J. Appl. Crystallogr.*, 2011, **44**, 1281-1284.

[24] L. J. Farrugia, WinGX and ORTEP for Windows: an update, *J. Appl. Crystallogr.*, 2012, **45**, 849-854.

[25] C. F. Macrae, P. R. Edgington, P. McCabe, E. Pidcock, G. P. Shields, R. Taylor, M. Towler and J. van De Streek, Mercury: visualization and analysis of crystal structures, *J. Appl. Crystallogr.*, 2006, **39**, 453–457.

[26] F. W. Küster, A. Thiel and E. Brückner, Tabelle per Le Analisi Chimiche e Chimico-fisiche. 14th ed., Hoepli, Milano, 1985, pp. 157-160.